Behavior of Benzene in Na-X and Na-Y Zeolites: Comparative Study by ^{2}H NMR and Molecular Mechanics

Scott M. Auerbach*

Departments of Chemistry and Chemical Engineering, University of Massachusetts, Amherst, Massachusetts 01003

Lucy M. Bull,[†] Neil J. Henson,[†,‡] Horia I. Metiu,[§,⊥] and Anthony K. Cheetham*[,†,‡,§]

Departments of Chemistry, Materials, Physics, and the Materials Research Laboratory, University of California, Santa Barbara, California 93106

Received: November 6, 1995; In Final Form: January 19, 1996[⊗]

We have performed solid state ^{2}H NMR spin−lattice relaxation measurements on perdeuterated benzene in the zeolites Na-X and Na-Y over the temperature range 155−350 K. The resulting NMR correlation times exhibit Arrhenius temperature dependence, with the following Arrhenius parameters: $\tau_0^Y = (9.6 \pm 0.4) \times 10^{-13}$ s, $E_a^Y = 23.5 \pm 0.9$ kJ mol^{-1}, $\tau_0^X = (8.8 \pm 2.3) \times 10^{-12}$ s, and $E_a^X = 14.0 \pm 0.6$ kJ mol^{-1}. This significant enhancement of benzene mobility from Na-Y to Na-X is reproduced with atomistic molecular mechanics simulations, yielding $E_a^Y = 35$ kJ mol^{-1} and $E_a^X = 15$ kJ mol^{-1}, in quite reasonable agreement with the NMR measurements. We propose a simple length scale model which accounts for both the mobility enhancement and its order of magnitude. We find that the enhancement from Na-Y to Na-X is due to attractive interactions from S_{III} sites influencing adjacent S_{II} sites, making mobility more energetically favorable in Na-X. The relative magnitudes of our calculated hopping activation energies suggest that, while intracage and intercage benzene mobilities are comparable in Na-X, intracage mobility is much more rapid than intercage migration for benzene in Na-Y.

I. Introduction

The transport properties of adsorbed molecules play a central role in catalytic and separation processes that take place within zeolite cavities.[1] Understanding the host−guest interactions that control molecular diffusion may suggest new materials with advanced performance. An important parameter characterizing the electrostatic environment of a zeolite is the Si:Al composition ratio, which ranges between one and infinity in different systems and which varies inversely with the density of exchangeable cations in the solid.[2] Molecular mobilities in high silica zeolites tend to decrease with decreasing Si:Al ratio,[3] especially for nucleophilic adsorbates which become trapped with long residence times at cationic sites.[3,4] To deepen our understanding of this trend, we test its applicability for low silica zeolites, which are important for chemical separation applications such as gas separation.[5] In the present study we use solid state NMR and molecular modeling techniques to determine how the Si:Al ratio controls benzene mobility in low silica faujasites.

In a previous article we reported solid state NMR measurements of benzene mobility in Na-Y(Si:Al=1.7) and siliceous faujasite, herein described as zero defect dealuminated-Y (ZDDAY).[6] Molecular dynamics (MD) calculations studying benzene mobility in ZDDAY were also reported.[6] The NMR and MD results for benzene in ZDDAY are consistent with vigorous intracage motion at all temperatures studied, and the calculations exhibit intercage migration above 400 K. The NMR results in Na-Y indicate that benzene is more confined than in ZDDAY, rotating only about its 6-fold axis. MD calculations for benzene in Na-Y[7,8] show that benzene is localized near Na(II) ions, in agreement with powder neutron diffraction[9] studies which show preferential sorption at the S_{II} site above Na(II). The room temperature NMR correlation times for benzene in ZDDAY and Na-Y are $(1.9 \pm 1.4) \times 10^{-10}$ and $(1.4 \pm 0.5) \times 10^{-8}$ s, respectively, completely consistent with the trend of decreasing mobility with decreasing Si:Al ratio. In the present paper we extend these studies to lower Si:Al ratios and find a *strong deviation* from this trend, with room temperature benzene mobilities increasing from Na-Y(Si:Al=1.7) to Na-X(Si:Al=1.2) by nearly 2 orders of magnitude.

We have developed a new zeolite−hydrocarbon potential energy surface (PES) and applied it to the calculation of binding energies and hopping activation energies for benzene in Na-Y(Si:Al=2.0).[10] These were used with the kinetic Monte Carlo method[11,12] to yield the first long length scale simulation of diffusion in cation-containing zeolites. Our calculations suggest that, in general, activation energies from long length scale diffusion measurements, e.g. pulsed field gradient (PFG) NMR, should be interpreted as site-to-window activation energies. Moreover, for benzene in Na-Y we predict that activation energies from NMR spin−lattice relaxation measurements correspond to *intracage* orientational randomization and, hence, should not agree with pulsed field gradient NMR results.

In the present study we extend this analysis to examine benzene mobility in Na-X(Si:Al=1.0) and Na-Y(Si:Al=2.0) by comparing calculated intracage and intercage hopping activation energies for the two systems. We find that the computational results agree qualitatively and semiquantitatively with the NMR measurements. Moreover, we propose a simple length scale model which accounts for the mobility enhancement and its order of magnitude, enabling the estimation of hopping activation energies in one system given those in another.

* Author to whom correspondence should be addressed.
[†] Materials Research Laboratory.
[‡] Department of Materials.
[§] Department of Chemistry.
[⊥] Department of Physics.
[⊗] Abstract published in *Advance ACS Abstracts,* March 15, 1996.

0022-3654/96/20100-5923$12.00/0

Finally, we predict that while NMR spin−lattice relaxation and PFG NMR are not expected to agree for benzene mobility in Na-Y, they *are* expected to agree for benzene in Na-X.

The remainder of the paper is as follows: in sections II and III we outline the experimental and theoretical methods. In section IV, we discuss the NMR results for benzene in Na-X and Na-Y in light of the expected mobility trend. In section V, we discuss the computational results and compare them with previously published experimental data. In section VI, we compare the measured and calculated results presented herein, and develop the length scale model of activation energies. Finally, in section VII we conclude.

II. Experimental Methodology

Na-X(Si:Al=1.2) was prepared by thoroughly mixing solutions of sodium aluminate and sodium metasilicate (SiO_2:Al_2O_3 = 2.5) with triethanolamine.[13] The resulting gel was transferred to a Teflon bottle, sealed, and then heated at 50 °C for 3 weeks. Na-Y(Si:Al=1.7) was purchased from Ventron Chemicals. The Si:Al ratios were determined by ^{29}Si MAS NMR.

Both samples were dehydrated under vacuum at 500 °C for at least 12 h before a known concentration of perdeuterated benzene (approximately 1 molecule per cavity) was added gravimetrically in a glovebox. The NMR samples were prepared in Pyrex ampules (5−10 mm o.d.), which, once loaded, were evacuated, keeping the zeolite at liquid N_2 temperature, and then flame sealed. The samples were heated at 80 °C for at least 4 h to attain a homogeneous distribution of sorbate within the sample.

Deuterium NMR spectra were recorded on Bruker MSL 300 and 400 spectrometers at frequencies of 46.05 and 61.4 MHz. Spin−lattice relaxation rates were measured using the inversion recovery method[14] followed by the quadrupole echo sequence for observation of the signal,[15] i.e. 180°−delay−$90°_x$−τ−$90°_y$−τ−echo. The 90° pulse was typically 3 μs, and the spin-echo delay, τ, 30 μs. Spectra were recorded as a function of temperature, allowing at least 30 min for the sample to reach thermal equilibrium. Temperatures were estimated to be accurate within ±2 K and were stable to ±0.5 K. A nonlinear least-squares (three parameter) fitting routine was used to calculate the values of T_1 from the τ dependence of the central peak intensity. No significant deviation from an exponential decay was observed, and it was therefore assumed that the motion causing the relaxation could be described by a single correlation time. Activation energies, quadrupole coupling constants (QCCs), and correlation times were obtained by fitting the temperature dependent T_1 data to the Bloembergen−Purcell−Pound (BPP) theory,[16] assuming isotropic motion. A full description of this data analysis has been given in an earlier paper.[6]

III. Theoretical Methodology

The zeolite−guest systems are represented as a collection of partially charged ions, interacting through short- and long-range forces. We replace Si and Al atoms with an average tetrahedral-site atom (T-atom) because of the difficulty in experimentally determining Al distributions in disordered zeolites. The charge on the average T-atom is determined by averaging Si and Al partial charges, according to the Si:Al ratio being considered. This approximation has been used in most molecular mechanics simulations of disordered zeolites. However, recent evidence[17] of Al and Si layering along the (111) plane in faujasite suggest that the average T-atom model may underestimate diffusive length scales and may totally neglect diffusive anisotropy. As more evidence characterizing Al distributions becomes available, it may be important to develop theoretical methods which relax the average T-site approximation.

For Na-Y we assume a Si:Al ratio of 2.0, requiring 64 Na ions per unit cell to balance charge. We assume full occupation of Na sites I′ (32 per unit cell, located in smaller β cages) and Na sites II (32 per unit cell, located in supercages). This occupancy model is reasonable considering that only the Na(II) ions are accessible to a penetrant the size of benzene. In addition, diffraction studies of Na-Y(Si:Al=1.7)[18] and -(Si:Al=2.4)[9] find nearly full Na(II) occupation.

For Na-X we assume a Si:Al ratio of 1.0, requiring 96 Na ions per unit cell. In this case we assume full occupation of Na sites I′ and II, as in the Na-Y model. The remaining 32 ions are distributed throughout Na(III) sites, which are generally found in the proximity of the 12-ring window. Several structures have now been reported for Na-X,[18−21] each differing in the precise locations of Na(III) ions. We adopt the structure of Hseu[19] which finds Na(III) binding four oxygens, two of which are in the 12-ring window. This structure is plausible and facilitates a simple model, with only one type of Na(III) site to occupy. Other structures[18,20,21] find some Na(III) closer to the plane of the 12-ring window, which might alter the balance between time scales for intracage and intercage motion.

There are 96 symmetry allowed Na(III) sites in the Hseu structure, but only 48 can be occupied simultaneously due to electrostatic repulsion. The partial S_{III} occupancy is assigned as follows. Of the six possible Na(III) sites in each supercage, which roughly fall on the edges of a tetrahedron and hence on the vertices of an octahedron, we occupy four sites on an equatorial plane of the octahedron. Although this occupancy is not fully symmetric, it does retain some symmetry. Indeed, this Na(III) occupancy scheme makes each Na(II) nearly identical, which greatly simplifies subsequent discussion of benzene hopping activation energies.

The PES we use has previously been described by us.[10] It was fitted to crystallographic[9] and thermochemical[22] data for benzene in Na-Y. In our present treatment of benzene in Na-X, the PES is unchanged, except that the T-atom partial charge becomes +1.9 when Si:Al = 1.0.

In order to quantify the effect of zeolite lattice relaxation on the energies of benzene sorption sites, we first relax the Na-X and Na-Y lattices without benzene, starting from crystallographic framework coordinates for Na-X[19] and Na-Y.[9] The resulting structures are then the starting point for benzene docking calculations. Comparing binding energies from energy minimizations with and without lattice relaxation allows us to determine the importance of such relaxation.

All energy minimizations are performed with our previously described MD-DOCKER algorithm.[10] In relaxing the Na-X structure, special care was taken to anneal the 32 Na(III) locations, requiring over 30 ps of high-temperature MD. During the MD runs, an interesting collective motion involving several Na(III) ions was discovered. We analyze this collective motion below and discuss its impact on benzene mobility in Na-X.

We model benzene mobility in Na-X and Na-Y by comparing calculated hopping activation energies for the two systems. Hopping activation energies control the temperature dependence of the NMR correlation times reported below. The activation energy is the difference between the transition state energy and the initial site energy. We locate the transition state for a particular hop by following the minimum energy path (MEP) from an initial site, through the transition state, to the final site. We calculate MEPs using a previously described constrained optimization approach,[10] which drags benzene from one site to another by constraining only a single component of the

benzene center of mass (COM), allowing all other coordinates to relax.

We depart from our previously described computational methodology[10] by defining a new hopping or "reaction" coordinate (RC). This new RC is more rigorous in that it is guaranteed to increase monotonically along the MEP. Since a reaction coordinate reduces a multidimensional space into a single coordinate, we must chose both the multidimensional space and the reduction procedure. For the multidimensional space, we consider both the 36-dimensional space of atomic coordinates (denoted collectively as R) and the 3-dimensional benzene center of mass (denoted by r). By comparing the RCs derived from these two spaces, we gain insight into orientational motion along benzene hopping paths.

We now give the reduction procedure. The center of mass RC definition follows easily once the full dimensional RC is defined, and as such, we focus on the latter. A full dimensional hopping path is the sequence of configurations $[R_0, R_1, R_2, ..., R_N]$. The partial hopping path length, L_n, is defined by $L_n = L_{n-1} + |R_n - R_{n-1}|$, where $L_0 = 0$. L_N is a discrete sum approximation to the integrated path length. The RC value for the configuration, Q_i, is given by $Q_i = L_i - L_N/2$, which implies $-Q_0 = L_N/2 = +Q_N$. The symmetry of benzene is taken into account in defining $|X - Y|$ by permuting over the atom indices to obtain the physically meaningful, shortest distance. In addition, $|X - Y|$ is normalized by the number of atoms in the benzene molecule. The center of mass RC, q, is obtained with the same algorithm, except using the 3-dimensional center of mass locations $[r_0, r_1, r_2, ..., r_N]$ and the usual 3-dimensional norm. The two RCs agree if a hopping path consists of only translational motion, and hence any difference between the two RCs signals reorientation along benzene hopping paths.

IV. Experimental Results and Discussion

Figure 1 compares the temperature dependence of the ^{2}H NMR spectra of C_6D_6 adsorbed in (a) Na-X(Si:Al=1.2) and (b) Na-Y(Si:Al=1.7). At 155 K both samples show an axially symmetric anisotropic powder pattern with a splitting between the singularities of ~66 MHz. This is typical of a rapid rotation of benzene around its 6-fold axis, which produces an effective quadrupole coupling constant with half the magnitude of that in the static molecule.[23] As the temperature is raised, the intensity at the center of the spectra associated with pseudo-isotropic motion, involving jumps among sets of sites where the orientations of the benzene 6-fold axis are related by tetrahedral[24] or higher symmetry, gradually dominates.

Quantitative measurements of the benzene correlation time have been obtained from ^{2}H NMR spin−lattice relaxation data. The results for the isotropic component of the C_6D_6 ^{2}H NMR line shape are shown in Table 1. Several observations can be made. First, the QCCs obtained from the BPP fit are intermediate between QCCs indicating pseudoisotropic motion and those indicating exclusively 6-fold rotation. This is typical when studying the crossover from one mobility regime to another.[6] Second, the two systems give very similar correlation time Arrhenius prefactors, indicating that the microscopic attempt frequencies for benzene hopping in Na-X and Na-Y are comparable. Third, and most striking, the activation energy for benzene in Na-Y is nearly twice that for benzene in Na-X. This result is somewhat counterintuitive: the most relevant chemical difference between Na-X and Na-Y is the number of Na ions accessible to benzene. Since Na-X contains more of these Na ions, and hence contains more sites which trap benzene for long residence times, how can the apparent activation energy for benzene mobility be lower in Na-X than in Na-Y? Bull has previously suggested that the Na(III) ions act as "stepping stones", facilitating benzene motion.[25] We can now sharpen this idea with the modeling results discussed below.

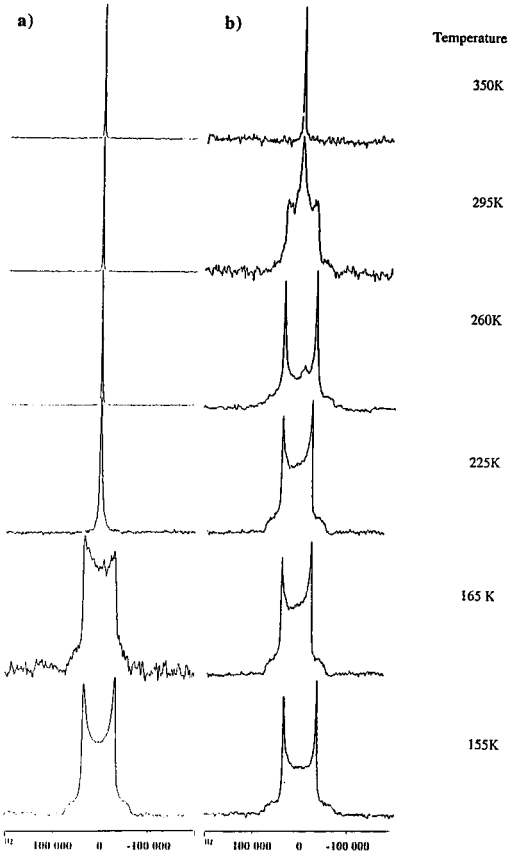

Figure 1. Temperature dependence of the ^{2}H NMR spectra of C_6D_6 adsorbed in (a) Na-X(Si:Al=1.2) and (b) Na-Y(Si:Al=1.7). The bottom spectra (155 K) indicate rapid rotation about the benzene 6-fold axis, while the top spectra (350 K) indicate pseudoisotropic motion.

TABLE 1: Parameters Resulting from Isotropic BPP Fit to Temperature Dependent NMR T_1 Data

BPP parameter	Na-Y(Si:Al=1.7)[a]	Na-X(Si:Al=1.2)[b]
E_a (kJ mol^{-1})	23.5 ± 0.9	14.0 ± 0.6
QCC (kHz)	47.3 ± 1.0	43.4 ± 0.9
τ_0 (s)	(9.6 ± 0.4) × 10^{-13}	(8.8 ± 2.3) × 10^{-12}
τ^{298} (s)	(1.4 ± 0.5) × 10^{-8}	(2.7 ± 1.3) × 10^{-9}

[a] Data collected at 61.4 MHz. [b] Data collected at 46.1 MHz.

V. Computational Results and Discussion

We now discuss the results of lattice optimizations for Na-X and Na-Y, docking calculations for benzene in Na-X and Na-Y, and hopping path calculations for benzene in the two zeolites. As mentioned above, our goal is to compare calculated hopping activation energies for benzene in Na-X and Na-Y.

A. Na-X and Na-Y Lattice Energy Minimization. We have relaxed the Na-Y(Si:Al=2.0) lattice with our zeolite potential, starting from the crystallographic structure of Fitch *et al.*[9] and our Na-Y occupancy model. The root mean square displacement of all Na-Y atoms is 0.2 Å, with no single atom moving more than 0.5 Å. We then relaxed the Na-X(Si:Al=1.0) lattice, starting from the crystallographic structure of Hseu[19] and our Na-X occupancy model. The root mean square displacement of all Na-X atoms is 0.34 Å, the additional 0.14 Å arising from 23 Na(III) ions jumping 1.5 Å across $Fd\bar{3}m$ mirror planes. (Although Na-X(Si:Al=1.0) has $Fd3$ symmetry, the average T-atom approach mimics the higher symmetry $Fd\bar{3}m$

TABLE 2: Optimized Binding Energies (kJ mol^{-1}) for Benzene Adsorbed in Na-X and Na-Y, with and without lattice relaxation

binding site	relaxed lattice	fixed lattice
Na-Y S_{II}	−77	−75
Na-Y W	−51	−50
Na-X S_{II}	−70	−68
Na-X S_{III}	−70	−69
Na-X W	−65	−64

structure.) In order to better understand this motion and its impact on benzene mobility, we discuss it in some detail.

There are three relevant Na-X configurations to consider: configuration I is the Hseu crystal structure,[19] configuration II results from MD-DOCKER relaxation starting from configuration I [run A = (10 cycles, 0.2 ps, 600 K)], and configuration II results from further MD-DOCKER relaxation, starting from configuration II [run B = (1 cycle, 10 ps, 600 K)]. Run A reduces the lattice energy by 5962 kJ mol^{-1} (31 kJ mol^{-1} per T-atom), and run B further reduces the energy by 28 kJ mol^{-1} (0.14 kJ mol^{-1} per T-atom). An additional MD-DOCKER calculation starting from configuration III [run C = (1 cycle, 20 ps, 600 K)] relaxes back to configuration III, suggesting that this may be the lowest energy Na-X structure. During run A, 14 Na(III) ions execute 1.5 Å jumps, while in run B 12 additional 1.5 Å jumps are made. Three Na(III) ions jump in both runs, returning in configuration III very near to their locations in configuration I. This suggests a double minimum energy structure for some or all Na(III) ions, the mobility of which could influence benzene mobility in Na-X.

We have performed a variety of additional optimizations to determine whether double minima exist for Na(III) ions. For example, we have placed one of the three ions which jump in both MD-DOCKER runs in its configuration II location, placed the rest of the system in configuration III, and relaxed the system. The special Na(III) ion falls back to its configuration III location, indicating the absence of a local double minimum for that ion. This suggests that the 1.5 Å jumps may require collective Na(III) motion. Long-range forces among Na(III) ions were found to be important when placing the special Na(III) in its configuration II location and annealing the locations of atoms within a sphere centered on the special Na(III). Only when the radius of the sphere exceeded 12 Å did the relaxation converge.

These results indicate that Na(III) motion promoting benzene mobility in Na-X is either energetically unfavorable for local ion motion or statistically improbable for collective ion motion. Even if these phenomena were to occur, they would only enhance benzene mobility if the activation energy for benzene motion in a fixed Na-X lattice exceeds 28 kJ mol^{-1}, since the collective ion motion from configuration III to configuration II is endoergic by that much energy. Below we find fixed lattice benzene hopping activation energies significantly lower than 28 kJ mol^{-1} all but ruling out Na(III) promotion of benzene mobility.

B. Benzene Docking in Na-X and Na-Y. After performing several MD-DOCKER calculations and analyzing the results with the Biosym/MSI visualization program INSIGHT,[26] we find two distinct binding sites for benzene in Na-Y, in agreement with the powder neutron diffraction results of Fitch *et al.*[9] In the S_{II} binding site, benzene is facially coordinated to a supercage 6-ring, 2.70 Å above Na(II). In the W site, benzene is centered in the 12-ring window, 5.3 Å from the S_{II} site. We calculated site binding energies with and without lattice relaxation, the results of which are summarized in Table 2. Because of the strong sodium−benzene interaction, the S_{II} site is much more stable than the W site. In both cases lattice relaxation stabilizes the system by only 1−2 kJ mol^{-1}, indicating that such relaxation is unimportant. These binding energies agree well with previously published experimental and theoretical values.[7,22,27,28] For a detailed comparison, please see ref 10.

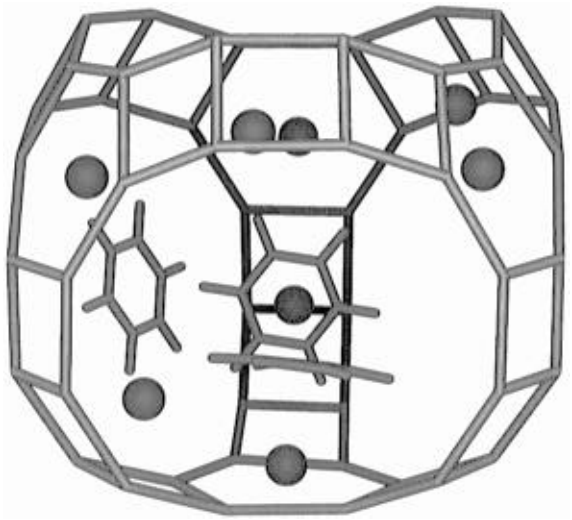

Figure 2. Calculated binding geometries for benzene in Na-X. Edge-on benzene at S_{II} site, 2.8 Å above Na(II), with −70 kJ mol^{-1} binding energy. Central benzene at S_{III} site, 2.8 Å above Na(III), with −70 kJ mol^{-1} binding energy. Left benzene at W site, with −65 kJ mol^{-1} binding energy.

TABLE 3: Distances between Optimized Binding Sites for Benzene Adsorbed in Na-X and Na-Y

binding site 1	binding site 2	distance (Å)
	Na-Y Sites	
S_{II}	S_{II}	5.5
S_{II}	W	5.3
W	W	8.8
	Na-X Sites	
S_{II}	S_{II}	6.1
S_{II}	W	5.7
S_{II}(close)	S_{III}	2.6
S_{II}(far)	S_{III}	4.0
S_{III}	W	4.4

After performing the above docking analysis for benzene in Na-X, we find S_{II} and W sites in addition to an S_{III} site over the Na(III) ion. In the S_{III} binding site, benzene is facially coordinated to a supercage 4-ring, 2.81 Å above Na(III). The binding geometries are shown in Figure 2, and the distances between sites are given in Table 3. Our calculated binding energies for benzene in Na-X, with and without lattice relaxation, are summarized in Table 2. The energies in Table 2 indicate a homogeneous binding environment for benzene in Na-X. Lattice relaxation stabilizes benzene in Na-X by only 1−2 kJ mol^{-1}, as we found for benzene in Na-Y. Indeed, because the faujasite supercage and 12-ring window are so large relative to benzene, framework flexibility is not expected to play a major role in our calculations. For these reasons, and those pertaining to the difficulty of Na(III) ions promoting benzene mobility (see above), the Na-X and Na-Y structures including Na ions are held rigid for the remaining calculations.

We now discuss how the Na(III) ions affect benzene binding in Na-X compared to that in Na-Y. Benzene in the Na-X S_{II} site is no longer parallel to the supercage 6-ring, as it is in Na-Y, because repulsive C_6H_5−H−Na(III) interactions distort the benzene plane orientation. The S_{II} site is less stable in Na-X than in Na-Y by 7 kJ mol^{-1}, and the sodium−benzene dis-

TABLE 4: Comparison between Measured and Calculated Heats of Sorption (kJ mol^{-1}) for Benzene Adsorbed in Na-X and Na-Y

study	Na-Y	Na-X
Barthomeuf[a]	78.7	73.2
Dzhigit[b]	79.5	83.5
present calc[c]	77	70

[a] Na-Y(Si:Al=2.43), Na-X(Si:Al=1.23), T = 445 K; ref 22. [b] Na-Y(Si:Al=2.27), Na-X(Si:Al=1.18), T = 323 K; ref 29. [c] Na-Y(Si:Al=2.00), Na-X(Si:Al=1.00), T = 0 K.

tance is longer in Na-X by 0.12 Å. Although the geometry of benzene in the Na-X W site is extremely similar to that in Na-Y, the Na-X W site is 14 kJ mol^{-1} more stable than in Na-Y, presumably due to favorable interactions with Na(III) ions ∼5 Å away. As such, our model predicts Na(III) destabilization of S_{II} sites and stabilization of W sites and hence a much larger population of benzene in the Na-X 12-ring window than in Na-Y.

To test our predictions further, we compare the calculated binding energies with measured heats of sorption for benzene in Na-X and Na-Y at infinite dilution. In order to make the most applicable comparison with experiment, we focus on Na-X and Na-Y measurements reported in the same study, to minimize complications from particle size and synthetic treatment effects. We are aware of two such studies, one by Barthomeuf *et al*.[22] and another by Dzhigit *et al*.[29] The comparison is shown in Table 4. The theoretically predicted destabilization of S_{II} binding by Na(III) ions suggests a lower heat of sorption for benzene in Na-X than in Na-Y. The heats measured by Barthomeuf *et al*. agree with this prediction, but interestingly the data from Dzhigit *et al*. do not. As such, there is no clear experimental trend on which to rely. The overall magnitudes of the heats agree reasonably well, which lends confidence to the modeling results. Further analysis of the experiments may be necessary before this trend is thoroughly understood.

C. Benzene Hopping Paths in Na-X and Na-Y. Destabilizing the Na-X S_{II} site by 7 kJ mol^{-1} above that in Na-Y gives a 15-fold enhancement of room temperature hopping processes originating at the S_{II} site, all other things being equal. To determine the full enhancement predicted by our PES, we calculated hopping paths and activation energies for benzene in Na-X and Na-Y.

A detailed analysis of benzene hopping paths in Na-Y has been given in an earlier paper,[10] in which the $S_{II} \rightarrow S_{II}$ jump was found to be the most efficient route to benzene orientational randomization (BOR). As such, the $S_{II} \rightarrow S_{II}$ hop is predicted to control NMR spin−lattice relaxation in this system. The minimum energy path for this jump is shown in Figure 3, along with the energetics in Figure 4. We denote this type of hopping process a "cartwheel" jump and predict an activation energy of 35 kJ mol^{-1}. Because this jump does not contribute to cage-to-cage mobility, the NMR correlation time should be interpreted simply as the mean residence time for benzene at the S_{II} site.

The presence of Na(III) ions in Na-X gives seven distinct benzene hopping paths to consider, of which we discuss four. The first is the $S_{II} \rightarrow S_{II}$ jump *without* a Na(III) between the two S_{II} sites, analogous to the Na-Y $S_{II} \rightarrow S_{II}$ pathway discussed above. For this jump we find the cartwheel mechanism shown in Figure 3, with a 25 kJ mol^{-1} activation energy, 10 kJ mol^{-1} lower than that in Na-Y. The decrease in activation energy arises mostly from the 7 kJ mol^{-1} destabilization of S_{II} sites in Na-X.

The next two hopping processes arise from the $S_{II} \rightarrow S_{II}$ jump *with* a Na(III) intermediate between the two S_{II} sites. This gives two distinct benzene jumps because Na(III) is not exactly in the middle between two S_{II} sites but, rather, is displaced from the mirror plane by ∼0.75 Å to either side. As such, there are two distinct benzene hopping activation energies. The apparent $S_{II} \rightarrow S_{III} \rightarrow S_{II}$ barrier is the larger of the two activation energies, unless Na(III) motion is rapid enough to promote benzene mobility *via* benzene−Na(III) hopping. The two benzene jumps are shown together in Figure 5, along with the energies in Figure 6, all with Na(III) held fixed. We denote the cartwheel jump in Figure 5 as the S_{II}(close) $\rightarrow S_{III}$ hop, which has a 6.4 kJ mol^{-1} activation energy. The remaining "gliding" motion is the $S_{III} \rightarrow S_{II}$(far) jump, which has a 15 kJ mol^{-1} activation energy. Since these calculated activation energies are much lower than that predicted for Na(III) motion ($E_a \geq$ 28 kJ mol^{-1}, see section VA), we predict that benzene−Na(III) motion is too sluggish to promote benzene mobility and, hence, that the 15 kJ mol^{-1} barrier controls the $S_{II} \rightarrow S_{III} \rightarrow S_{II}$ process. With four of six Na(III) sites populated in our model, benzene can reach all four S_{II} sites by making $S_{II} \rightarrow S_{III} \rightarrow S_{II}$ jumps. Thus, we predict the *intracage* BOR is controlled by the 15 kJ mol^{-1} $S_{III} \rightarrow S_{II}$(far) barrier.

Hopping processes which contribute to *intercage* migration, and hence diffusion, may also be efficient routes to BOR. We investigated this for benzene in Na-X by calculating the $S_{III} \rightarrow$ W activation energy. The hopping path is shown in Figure

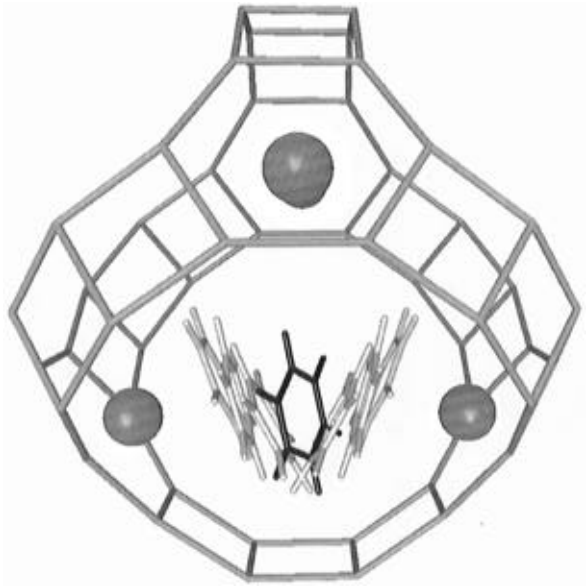

Figure 3. Calculated $S_{II} \rightarrow S_{II}$ minimum energy path for benzene in Na-Y, exhibiting "cartwheel" mechanism with transition state in bold. Calculated activation energy is 35 kJ mol^{-1}. Similar jump for benzene in Na-X has 25 kJ mol^{-1} activation energy.

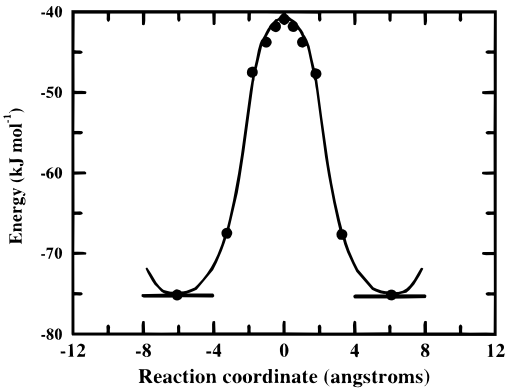

Figure 4. Calculated $S_{II} \rightarrow S_{II}$ hopping path energies for benzene in Na-Y, showing 35 kJ mol^{-1} activation energy.

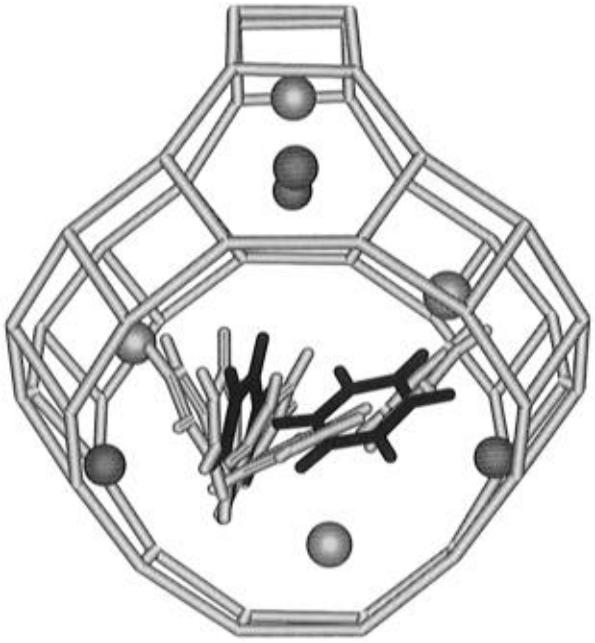

Figure 5. Calculated $S_{II} \rightarrow S_{II}$ *via* S_{III} minimum energy path for benzene in Na-X. Cartwheel S_{II}(close) $\rightarrow S_{III}$ hop on left has 6.4 kJ mol^{-1} activation energy, while the gliding $S_{III} \rightarrow S_{II}$(far) jump on the right controls intracage mobility with 15 kJ mol^{-1} activation energy.

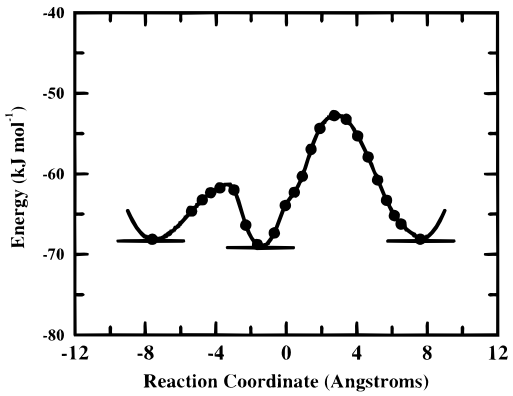

Figure 6. Calculated $S_{II} \rightarrow S_{II}$ *via* S_{III} hopping path energies for benzene in Na-X, showing 6.4 and 15 kJ mol^{-1} activation energies.

7, and the energies are shown in Figure 8. This is a cartwheel jump with a late barrier, very similar to the $S_{II} \rightarrow W$ jump in Na-Y.[10] The calculated activation energy for this process is also 15 kJ mol^{-1}, suggesting that intracage BOR and intercage BOR may exhibit very similar time scales for benzene in Na-X.

This has interesting implications for the predicted agreement between NMR spin−lattice relaxation and PFG NMR measurements of benzene mobility in Na-X and Na-Y. Since our calculated activation energies for benzene in Na-Y suggest that BOR is controlled by intracage motion, an NMR spin−lattice relaxation measurement would not probe diffusive, intercage motion and, hence, should not agree with the results of a PFG NMR experiment. Alternatively, since the calculated activation energies for intracage BOR and intercage BOR are comparable in Na-X, we predict that NMR spin−lattice relaxation and PFG NMR measurements of benzene in Na-X are likely to yield similar results. Indeed, for benzene in Na-X at low coverage, the ^{2}H NMR line width results of Burmeister *et al.*[30] agree quite reasonably with the PFG NMR measurements of Germanus *et al.*,[31] yielding activation energies of 22.5 and 20 kJ mol^{-1}, respectively. These experimental results also agree reasonably well with our 15 kJ mol^{-1} calculated activation energy.

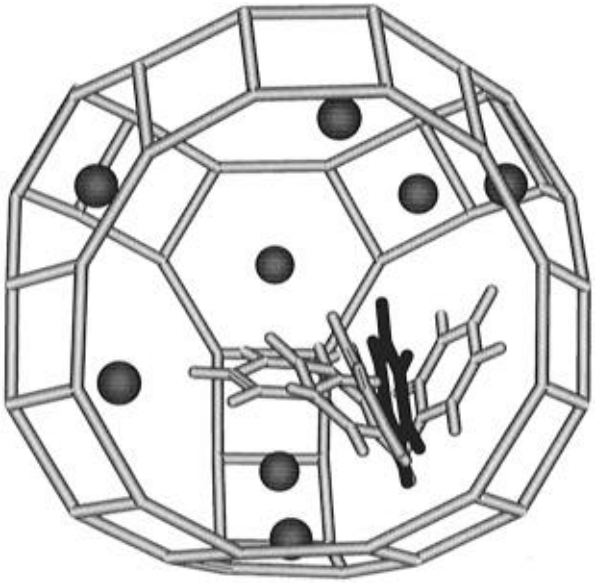

Figure 7. Calculated $S_{III} \rightarrow W$ minimum energy path for benzene in Na-X. Cartwheel hop controls intercage mobility and has 15 kJ mol^{-1} activation energy.

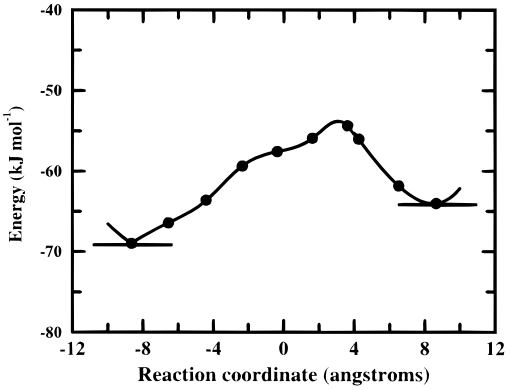

Figure 8. Calculated $S_{III} \rightarrow W$ hopping path energies for benzene in Na-X, showing 15 kJ mol^{-1} activation energy.

TABLE 5: Summary of Calculated Hopping Activation Energies (kJ mol^{-1}) for Benzene in Na-X and Na-Y

zeolite	jump	activation energy
Na-Y	$S_{II} \rightarrow S_{II}$	35[a]
Na-Y	$S_{II} \rightarrow W$	41[b]
Na-X	$S_{II} \rightarrow S_{II}$	25
Na-X	S_{II}(close) $\rightarrow S_{III}$	6.4
Na-X	$S_{III} \rightarrow S_{II}$(far)	15[a]
Na-X	$S_{III} \rightarrow W$	15[b]

[a] Controls intracage benzene orientational randomization. [b] Controls intercage benzene diffusion.

Although a direct comparison is not yet available for benzene in Na-Y, experiments are underway to address this issue.

In addition to giving activation energies, the hopping paths provide detailed mechanistic information about benzene mobility. For example, the full dimensional and center of mass reaction coordinates defined above help to illustrate the importance of reorientation along benzene hopping paths. When plotting one reaction coordinate against another for a given hopping process, a nonlinear portion of the plot signals benzene reorientation. Figure 9 shows this for the $S_{II} \rightarrow S_{III} \rightarrow S_{II}$ composite hop. The portion of the curve corresponding to the S_{II}(close) $\rightarrow S_{III}$ jump is very nonlinear, reflecting benzene reorientation during the cartwheel process. On the other hand, most of the $S_{III} \rightarrow S_{II}$(far) portion of the curve is linear, indicating that the gliding process is exclusively center of mass

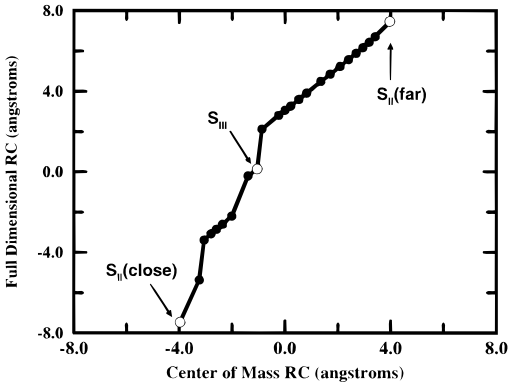

Figure 9. Comparison of calculated reaction coordinates shows S_{II}(close) → S_{III} curve is nonlinear, reflecting benzene reorientation during cartwheel process. S_{III} → S_{II}(far) curve is linear, indicating that gliding process is center of mass motion.

motion. In general, we find this reaction coordinate analysis a useful tool for picturing complicated hopping motions.

VI. Comparison between Experiment and Theory

As discussed above in section V, there is quite reasonable agreement between the results of our calculations and those of previously published experiments. Now we compare the experimental and computational results presented above, with the assumption that the NMR spin−lattice relaxation measurements probe BOR.

For benzene in Na-Y, we predict a 35 kJ mol^{-1} activation energy for BOR, as compared with the experimental value of 23.5 ± 0.9 kJ mol^{-1}. Two sources may contribute to this discrepancy. First, the potential energy surface is approximate and can be refined by performing quantum cluster calculations on the stable S_{II} site[28] and the transition state suggested by our molecular mechanics calculations. Second, we are comparing measurements for benzene in Na-Y(Si:Al=1.7) and calculations for benzene in Na-Y(Si:Al=2.0). Diffraction studies of Na-Y(Si:Al=1.7)[18] observe Na(III) occupation, on the order of one per supercage. This Na(III) ion may destablize benzene at two of the four S_{II} sites, while lying along only one of the six S_{II} → S_{II} hopping paths. As such, it may be more appropriate to compare the experimental value of 23.5 ± 0.9 kJ mol^{-1} to the hopping activation energy for the Na-X S_{II} → S_{II} jump *without* a Na(III) between, which is predicted to be 25 kJ mol^{-1}. Further calculations are underway to resolve these issues.

For benzene in Na-X, we predict a 15 kJ mol^{-1} activation energy for BOR, in excellent agreement with the experimental value of 14.0 ± 0.6 kJ mol^{-1}. In light of the possible discrepancy noted above for benzene in Na-Y, the close agreement for benzene in Na-X may be fortuitous. Nevertheless, the intriguing trend of increasing benzene mobility from Na-Y to Na-X is well-reproduced by the potential energy surface and modeling procedures. This is remarkable considering that although the potential energy surface was fit to heats of sorption and low-temperature crystallography of benzene in Na-Y,[10] the modeling results are consistent with a wider variety of phenomena.

To fully understand the enhancement of benzene mobility from Na-Y to Na-X, we propose a simple model which accounts for both the enhancement and its order of magnitude. The most relevant difference between Na-X and Na-Y is the number of Na ions accessible to benzene. Na-X contains more of these Na ions and, hence, contains more sites which trap benzene. Adding a new sorption site can have three different effects on mobility. First, if the new site binds very weakly, mobilities will be largely unchanged. Second, if the new site binds much more strongly than already existing sites, mobilities will be decreased. Third, if both sites are affected so that both bind as tightly, mobilities will be enhanced. We use a simple length scale argument to predict which situation is expected. The Na(II)−benzene center of mass distance in Na-Y is 2.70 Å.[9] The ionic radius of Na is 0.97 Å,[32] while the graphite layer distance is 3.35 Å.[32] Using these parameters, a Na(II)−benzene packing distance is estimated to be 2.65 Å, a value slightly less than the observed distance. This suggests that there is very little steric repulsion imposed by the zeolite framework at the S_{II} site. The proximity of Na(III) to the large 12-ring windows suggests an even smaller framework steric effect at the S_{III} site. As such, we expect the S_{II} and S_{III} binding strengths to be very comparable, pointing to the enhancement of benzene mobility from Na-Y to Na-X.

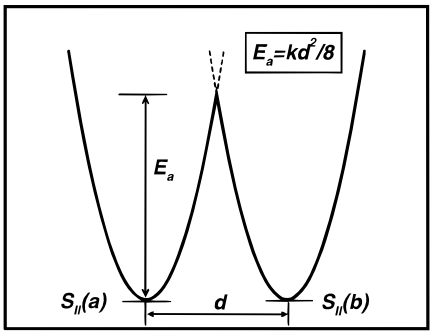

Figure 10. One dimensional harmonic model of adjacent S_{II} sites in Na-Y, parametrized as $V_a(x) = {}^1/_2kx^2$ and $V_b(x) = {}^1/_2k(x - d)^2$, with d = 5.5 Å. k was obtained by equating parabola intersection energy ${}^1/_2k(d/2)^2$ with hopping barrier E_a.

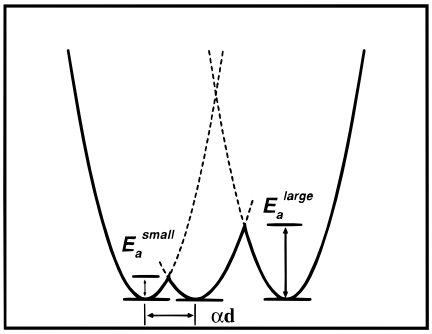

Figure 11. Na-Y model of adjacent S_{II} sites applied to Na-X, which adds the S_{III} site parametrized as $V_c(x) = {}^1/_2k(x = \alpha d)^2$ with $\alpha = 0.35$. The resulting two activation energies are α^2E_a and $(1 - \alpha)^2E_a$.

This qualitative length scale argument can be extended to quantitatively account for the mobility enhancement from Na-Y to Na-X. We assume a one dimensional harmonic model of adjacent S_{II} sites in Na-Y, illustrated in Figure 10. The oscillators are parametrized as $V_a(x) = {}^1/_2kx^2$ and $V_b(x) = {}^1/_2k(x - d)^2$. The values of d and k can be extracted from either experimental or theoretical data for benzene in Na-Y. In either case, d = 5.5 Å, and k is determined by setting the parabola intersection energy ${}^1/_2k(d/2)^2$ equal to the hopping activation energy E_a, which is 23.5 ± 0.9 kJ mol^{-1} experimentally and 35 kJ mol^{-1} theoretically. Introducing Na(III) adds a new site, which in our present model adds the harmonic well $V_c(x) = {}^1/_2k(x - \alpha d)^2$, shown in Figure 11, where by symmetry α is between zero and one-half. Na-X thus has two distinct activation energies calculated at the intersections of $V_a(x)$ with $V_c(x)$ and $V_b(x)$ with $V_c(x)$. These are given by $E_a^{\text{small}} = \alpha^2E_a$, and $E_a^{\text{large}} = (1 - \alpha)^2E_a$. Table 3 suggests $\alpha = 0.35$, which is obtained by projecting the Na-X distances $d(S_{II}(\text{close}),S_{III})$ = 2.6 Å and $d(S_{III},S_{II}(\text{far}))$ = 4.0 Å onto a line 5.5 Å long. The

TABLE 6: Comparison between Measured, Calculated, and Estimated Activation Energies (kJ mol^{-1}) for Benzene Mobility in Na-X

method	E_a^{small}	E_a^{large}
measured		14.0 ± 0.6
calculated	6.4	15
estimated from Na-Y measurements	2.9	9.9
estimated from Na-Y calculations	4.3	15

results of this analysis are shown in Table 6. Using this value of α and the calculated Na-Y barrier, we obtain excellent agreement with the calculated Na-X barriers. Using this value of α and the measured Na-Y barrier, we obtain an E_a^{large} value somewhat lower than the measured Na-X barrier. Nevertheless, the generally good agreement between Na-X barriers estimated from Na-Y data, and those obtained directly from Na-X, suggest that the observed mobility enhancement derives simply from overlapping sorption sites. We find it remarkable that such a simple model can quantitatively account for this effect.

VII. Conclusions

We have performed solid state ^{2}H NMR spin−lattice relaxation measurements on perdeuterated benzene in the zeolites Na-X and Na-Y over the temperature range 155−350 K. We interpret the correlation times extracted from the NMR measurements as time scales for benzene orientational randomization. The correlation times exhibit Arrhenius temperature dependence, with the following Arrhenius parameters: $\tau_0^Y = (9.6 \pm 0.4) \times 10^{-13}$ s, $E_a^Y = 23.5 \pm 0.9$ kJ mol^{-1}, $\tau_0^X = (8.8 \pm 2.3) \times 10^{-12}$ s, and $E_a^X = 14.0 \pm 0.6$ kJ mol^{-1}. This represents a significant enhancement of benzene mobility from Na-Y to Na-X, which we find intriguing considering that Na-X contains more sites which trap benzene.

We reproduce the enhancement effect with atomistic molecular mechanics simulations, based on a previously described potential energy surface. The calculations yield $E_a^Y = 35$ kJ mol^{-1} and $E_a^X = 15$ kJ mol^{-1}, in quite reasonable agreement with the NMR measurements. We propose a simple length scale model which accounts for both the mobility enhancement and its order of magnitude. We find that the enhancement from Na-Y to Na-X is due to attractive interactions from S_{III} sites overlapping those from adjacent S_{II} sites, making mobility more energetically favorable in Na-X. This model is significant because it allows us to use data from one zeolite system to estimate activation energies for other zeolite systems. On the basis of the relative magnitudes of our calculated intracage and intercage hopping activation energies, we predict that while NMR spin−lattice relaxation and PFG NMR are expected to agree for benzene mobility in Na-X, they are not expected to agree for benzene in Na-Y.

Acknowledgment. S.M.A. acknowledges support from the National Science Foundation (NSF) under Grant CHE-9403159, and from Biosym/MSI for the use of visualization software. N.J.H. and A.K.C. thank Los Alamos National Laboratory and Biosym/MSI for financial support. H.I.M. acknowledges the NSF and the Office of Naval Research for funding. This work was partially funded by the UCSB-MRL which is supported by the NSF under Award No. DMR-9123048.

References and Notes

(1) Kärger, J.; Ruthven, D. M. *Diffusion in Zeolites and Other Microporous Solids*; Wiley: New York, 1992.
(2) Newsam, J. M. Zeolites. In *Solid State Chemistry: Compounds*; Cheetham, A. K., Day, P., Eds.; Oxford University Press: Oxford, U.K., 1992; pp 234−280.
(3) Uytterhoven, L.; Dompas, D.; Mortier, W. J. *J. Chem. Soc., Faraday Trans.* **1992**, *88*, 2753.
(4) Klein, H.; Kirschhock, C.; Fuess, H. *J. Phys. Chem.* **1994**, *98*, 12345.
(5) Yang, R. T. *Gas Separation by Adsorption Processes*; Butterworth: Stoneham, MA, 1987.
(6) Bull, L. M.; Henson, N. J.; Cheetham, A. K.; Newsam, J. M.; Heyes, S. J. *J. Phys. Chem.* **1993**, *97*, 11776.
(7) Demontis, P.; Yashonath, S.; Klein, M. L. *J. Phys. Chem.* **1989**, *93*, 5016.
(8) Henson, N. J. Ph.D. Thesis, Oxford University, 1995.
(9) Fitch, A. N.; Jobic, H.; Renouprez, A. *J. Phys. Chem.* **1986**, *90*, 1311.
(10) Auerbach, S. M.; Henson, N. J.; Cheetham, A. K.; Metiu, H. I. *J. Phys. Chem.* **1995**, *99*, 10600.
(11) Fichthorn, K. A.; Weinberg, W. H. *J. Chem. Phys.* **1991**, *95*, 1090.
(12) June, R. L.; Bell, A. T.; Theodorou, D. N. *J. Phys. Chem.* **1991**, *95*, 8866.
(13) Charnell, J. F. *J. Cryst. Growth* **1971**, *8*, 291.
(14) Hahn, E. L. *Phys. Rev.* **1949**, *76*, 145.
(15) Davis, J. H.; Jeffrey, K. R.; Bloom, M.; Valic, M. I.; Higgs, T. P. *Chem. Phys. Lett.* **1976**, *42*, 390.
(16) Bloembergen, N.; Purcell, E. M.; Pound, R. V. *Phys. Rev.* **1948**, *73*, 679.
(17) Alfredsson, V.; Terasaki, O.; Blum, Z.; Bovin, J. O. *Zeolites* **1995**, *15*, 111.
(18) Eddy, M. M. Ph.D. Thesis, Oxford University, 1985.
(19) Hseu, T. Ph.D. Thesis, University of Washington, 1972.
(20) Olson, D. H. *Zeolites* **1995**, *15*, 439.
(21) Vitale, G.; Bull, L. M.; Cheetham, A. K. Manuscript in preparation.
(22) Barthomeuf, D.; Ha, B. H. *J. Chem. Soc., Faraday Trans. 1* **1973**, *69*, 2147.
(23) Nishikiori, S.; Ratcliffe, C. I.; Ripmeester, J. A. *J. Phys. Chem.* **1991**, *95*, 1589.
(24) Wilhelm, M.; Firouzi, A.; Favre, D. E.; Bull, L. M.; Schaefer, D. J.; Chmelka, B. F. *J. Am. Chem. Soc.* **1995**, *117*, 2923.
(25) Bull, L. M. Ph.D. Thesis, Oxford University, 1993.
(26) *InsightII User Guide*, version 2.3.0; Biosym Technologies: San Diego, CA, 1994.
(27) Henson, N. J.; Cheetham, A. K.; Stockenhuber, M.; Lercher, J. A. Manuscript in preparation.
(28) O'Malley, P. J.; Braithwaite, C. J. *Zeolites* **1995**, *15*, 198.
(29) Dzhigit, O. M.; Kiselev, A. V.; Rachmanova, T. A. *Zeolites* **1984**, *4*, 389.
(30) Burmeister, R.; Schwarz, H.; Boddenberg, B. *Ber. Bunsen-Ges. Phys. Chem.* **1989**, *93*, 1309.
(31) Germanus, A.; Kärger, J.; Pfeifer, H.; Samulevic, N. N.; Zdanov, S. P. *Zeolites* **1985**, *5*, 91.
(32) Atkins, P. W. *Physical Chemistry*; Oxford University Press: Oxford, U.K., 1993.

JP953260P